Submitted to

32nd International Conference on High Energy Physics, ICHEP04, August 16, 2004, Beijing

Abstract: **5-0167**

Parallel Session **5**

www-h1.desy.de/h1/www/publications/conf/conf_list.html

Measurement of $F_2^{c\bar{c}}$ and $F_2^{b\bar{b}}$ at High Q^2 using the H1 Vertex Detector at HERA

H1 Collaboration

Abstract

Measurements are presented of inclusive charm and beauty cross sections in e^+p collisions for values of $Q^2 > 110$ GeV^2 and $0.05 < y < 0.7$, using a method based on the distance of closest approach, in the transverse plane, of tracks to the primary vertex as measured by the H1 vertex detector. The data are divided into four intervals in Q^2 and Bjorken x and values for the structure functions $F_2^{c\bar{c}}$ and $F_2^{b\bar{b}}$ are obtained. The results are found to be compatible with the predictions of perturbative quantum chromodynamics.

1 Introduction

Heavy quark production is an important process to study quantum chromodynamics (QCD). It is expected that perturbative QCD (pQCD) at next-to-leading order (NLO) should give a good description of heavy flavour production in deep-inelastic scattering (DIS), especially at values of the negative square of the four momentum of the exchanged boson Q^2 greater than the square of the heavy quark masses. Measurements of the open charm (c) cross section in DIS at HERA have mainly been of exclusive D or D^* meson production[1, 2]. The contribution of charm to the proton structure function, $F_2^{c\bar{c}}$, is derived by correcting for the fragmentation fraction $f(c \to D)$ and the unmeasured phase space (mainly at low values of transverse momentum of the meson). The results have been found to be in good agreement with QCD predictions. The measurement of the beauty (b) cross section is particularly challenging since b events comprise only a small fraction (typically $< 5\%$) of the total cross section. The b cross section has been measured in DIS ($Q^2 > 2\ \mathrm{GeV}^2$) by ZEUS[3] and in photoproduction ($Q^2 \simeq 0\ \mathrm{GeV}^2$) by H1[4] and ZEUS[5], using the transverse momentum distribution of muons relative to the b jet in semi-muonic decays. Measurements of the b cross section have also been made in $p\bar{p}$[6] and $\gamma\gamma$ collisions[7].

The analysis presented in this paper is of inclusive c and b cross sections in e^+p scattering at HERA in the range $Q^2 > 110\ \mathrm{GeV}^2$. Events containing heavy quarks can be distinguished from light quark events by the long lifetimes of c and b hadrons, which lead to displacements of tracks from the primary vertex. The contribution of light quark events with long lived decays may be reduced by restricting the size of the maximum allowed displacements. The distance of a track to the primary vertex is reconstructed using precise spatial information from the H1 vertex detector. The lifetimes of the heavy mesons and the quark fragmentation functions are taken from measurements made by other experiments[8]. The results presented in this paper are made in kinematic regions where there is little extrapolation needed to correct to the full phase space. The charm structure function $F_2^{c\bar{c}}$ and the corresponding structure function for b quarks $F_2^{b\bar{b}}$ are obtained after small corrections for the longitudinal structure functions $F_L^{c\bar{c}}$ and $F_L^{b\bar{b}}$ (taken from NLO predictions). This is the first measurement of $F_2^{b\bar{b}}$ and an extension to high Q^2 of previous H1 $F_2^{c\bar{c}}$ measurements.

2 Heavy Flavour Production

In pQCD, in the region where Q^2 is much larger than the squared mass M^2 of the heavy flavour quark, the production of heavy flavour quarks is expected to be insensitive to threshold effects and the quarks may be treated as massless partons. At leading order (LO), in the 'massless' scheme, the quark parton model (QPM) process ($\gamma q \to q$) is the dominant contribution. At NLO, the photon gluon fusion ($\gamma g \to q\bar{q}$) and QCD Compton ($\gamma q \to qg$) processes also contribute. The approach is often referred to as the zero mass variable flavour number scheme (ZM-VFNS)[9, 10].

At values of $Q^2 \sim M^2$, the 'massive' scheme[11], in which the heavy flavour partons are treated as massive quarks is more appropriate. The heavy quarks are produced perturbatively with their mass providing the hard scale. The dominant LO process is photon gluon fusion

(PGF) and the NLO diagrams are of order α_s^2. The scheme is often referred to as the fixed flavour number scheme (FFNS). As Q^2 becomes large compared to M^2, the FFNS approach is unreliable due to large logarithms in $\ln(Q^2/M^2)$, which lead to a divergence in the perturbative series.

In order to provide reliable pQCD predictions for the description of heavy flavour production, over the whole range in Q^2, composite schemes which provide a smooth transition from the massive description at $Q^2 \sim M^2$ to the massless behaviour at $Q^2 \gg M^2$ have been developed[12, 13]. The scheme is commonly referred to as the variable flavour number scheme (VFNS). The approach has been incorporated in various different forms to order α_s[12] and to order α_s^2[13].

3 H1 Detector

Only a short description of the H1 detector is given here; a full description may be found in[14]. A right handed coordinate system is employed at H1 that has its z-axis pointing in the proton beam, or forward, direction and $x(y)$ pointing in the horizontal(vertical) direction.

Charged particles are measured in the central tracking detector (CTD). This device consists of two cylindrical drift chambers interspersed with z-chambers to improve the z-coordinate reconstruction and multi–wire proportional chambers mainly used for triggering. The CTD is situated in a uniform $1.15\,\mathrm{T}$ magnetic field, enabling momentum measurement of charged particles over the pseudo-rapidity range $-1.74 < \eta < 1.74$ [1].

The CTD tracks are linked to hits in the vertex detector (central silicon tracker CST)[15], to provide precise spatial track reconstruction. The CST consists of two cylindrical layers of double-sided silicon strip detectors surrounding the beam pipe, covering a pseudo-rapidity range of $-1.32 < \eta < 1.32$. This detector provides hit resolutions of 12μm in r–ϕ and 25μm in z. For CTD tracks with CST hits in both layers the transverse distance of closest approach to the nominal vertex in x–y can be measured with a resolution of $33\ \mu\mathrm{m} \oplus 90\ \mu\mathrm{m}/p_T[\mathrm{GeV}]$, where the first term represents the intrinsic resolution (including alignment uncertainty) and the second term is the contribution from multiple scattering in the beam pipe and the CST; p_T is the transverse momentum of the track. In this analysis, the measurement of the z coordinate by the CST is not used for determining the distance of closest approach of a track.

The track detectors are surrounded in the forward and central directions ($-1.5 < \eta < 3.4$) by a fine grained liquid argon calorimeter (LAr) and in the backward region ($-4.0 < \eta < -1.4$) by a lead–scintillating fibre calorimeter[16] with electromagnetic and hadronic sections. These calorimeters provide energy and angular reconstruction for final state particles from the hadronic system. The LAr is also used in this analysis to measure and identify the scattered positron.

An electromagnetic calorimeter situated downstream in the positron beam direction measures photons from the bremsstrahlung process $ep \rightarrow ep\gamma$ for the purpose of luminosity determination.

[1] The pseudo-rapidity ($\eta = -\ln\tan\theta/2$) coverage of each detector component is given for the vertex in its nominal position.

4 Experimental Method

The analysis is based on a high Q^2 sample of neutral current (NC) events, taken in the years 1999-2000, when HERA was operated in unpolarised e^+p mode, with an ep centre of mass energy squared $s = 101200\ \mathrm{GeV}^2$. The events are selected in a similar manner to that described in[17]. Additional requirements are made on the performance of the CTD, yielding an integrated luminosity of 57.4 pb^{-1}. The positron is identified and measured in the LAr calorimeter, which restricts the measurement to $Q^2 > 110\ \mathrm{GeV}^2$. The event kinematics Q^2 and the inelasticity variable y are reconstructed using the scattered positron. The Bjorken scaling variable x is obtained from $x = Q^2/sy$. After the inclusive selection the total number of events is around 121,000.

4.1 Monte Carlo Simulation

The data are corrected for the effects of detector resolution, acceptance and efficiency by the use of Monte Carlo simulations. The Monte Carlo program RAPGAP [19] is used to generate high Q^2 NC DIS events for the processes $ep \rightarrow eb\bar{b}X$, $ep \rightarrow ec\bar{c}X$ and light quark production. RAPGAP combines $\mathcal{O}(\alpha_s)$ matrix elements with higher order QCD effects modelled by the emission of parton showers. The heavy flavour event samples are generated according to the massive PGF matrix element with the mass of the c and b quarks set to $m_c = 1.5$ GeV and $m_b = 5.0$ GeV, respectively. The partonic system is fragmented according to the LUND string model implemented within the JETSET program [20]. The HERACLES program [21] is used to calculate single photon radiative emissions off the lepton line and virtual electroweak corrections. In the event generation, the DIS cross section is calculated with a LO parton density function (PDF) in the DIS scheme [10]. In order to improve the description of the data by the simulation, the simulated cross sections are reweighted in x and Q^2 using a NLO QCD fit (H1 PDF2000) to the H1 data [17].

The samples of events generated for the uds, c, and b processes are passed through a detailed simulation of the detector response based on the GEANT3 program [18], and through the same reconstruction software as is used for the data.

4.2 Track, Vertex and Jet Reconstruction

The analysis is based on CTD tracks which are linked to r–ϕ hits in both planes of the CST in order to improve the precision of the track parameters. In this paper, the CST-improved CTD tracks are referred to as 'CST tracks'. Only those events which have at least 1 reconstructed CST track with polar angle $30 < \theta_{\text{track}} < 150^\circ$ and a minimum transverse momentum of 0.5 GeV are used. The reconstructed z position of the interaction vertex must be within ± 20 cm of the centre of the detector to match the acceptance of the CST. At low values of y, the hadronic final state (HFS) tends to go forward and outside the acceptance of the CST. Therefore, the analysis is restricted to $0.07 < y < 0.7$. The upper y cut ensures a good trigger acceptance for the scattered positron. In this kinematic range, studies from Monte Carlo simulations show that 93% of c events and 96% of b events are expected to have at least one charged particle, with a $p_T > 0.5$ GeV in the angular range $30 < \theta < 150°$, produced from the decay of a heavy hadron. The restriction to this kinematic range thus ensures that the extrapolation to the full phase space, needed to calculate $F_2^{c\bar{c}}$ and $F_2^{b\bar{b}}$, is small.

The efficiency for a single charged particle with $p_T > 0.5$ GeV to produce a CST track varies between 60% and 75% depending on the z position of the track in the CST. The polar angle and transverse momentum distributions of CST tracks are compared to the Monte Carlo simulation in figure 1. The simulation gives a reasonable description of these distributions.

The primary event vertex in r–ϕ is reconstructed from all tracks (with or without CST hits) and the position and spread of the beam interaction region (referred to as the 'beam-spot'). The beam-spot extension is measured to be $\sim 145\ \mu\mathrm{m}$ in x and $\sim 25\ \mu\mathrm{m}$ in y for the data period considered here. The position of the beam-spot is measured as the average over many events and the resulting error on the position is small in comparison to the size of the beam-spot, with a typical uncertainty of $\sim 5\ \mu\mathrm{m}$.

In this analysis the transverse distance of closest approach (DCA) of the track to the primary vertex point is used to separate the different quark flavours (see section 4.3). The uncertainty of the measurement of the DCA receives contributions from the position of the primary vertex discussed above, the intrinsic resolution of the track and distortions due to multiple scattering in the beam-pipe and surrounding material. In order to provide a successful description of the DCA in the data by the Monte Carlo simulation program, the Monte Carlo parameters for the beam-spot size, tracking resolution and inactive material are adjusted to those observed in the data.

To identify long lived hadrons a 'jet axis' is defined for each event in order to calculate a signed DCA for every track. Jets with a minimum p_T of 5 GeV, in the angular range $10^{\circ} < \theta < 170^{\circ}$, are reconstructed using the invariant k_T algorithm[22] run in the laboratory frame over all reconstructed HFS particles. HFS particles are reconstructed using a combination of tracks and calorimeter energy deposits[23]. The jet axis is defined as the direction of the jet with the highest transverse momentum or, if there is no jet reconstructed in the event, as the direction of the struck quark in the quark parton model [24] as reconstructed from the scattered electron and HFS particles. In the Q^2 range of this paper, the vector sum of all HFS particles in the laboratory frame always has a transverse momentum greater than 5 GeV and 97% of the events have the jet axis defined by a reconstructed jet.

CST tracks are associated to the jet axis if they lie within a cone of size 1 in η–ϕ space centred about the jet axis. Approximately 65% of events within the kinematic range have at least one CST track which is matched to the jet axis. Figure 2 shows the polar angle and p_T distributions of the jets which contain one or more CST tracks. Figure 3 shows the number of reconstructed CST tracks assigned to the jet axis. The simulation gives a reasonable description of these distributions. The deviations observed at high track multiplicities are most likely due to an incomplete description of light quark multiplicities in the Monte Carlo. This has negligible effect on the measurements.

4.3 Quark Flavour Separation

The different quark flavours that contribute to the DIS cross section are distinguished on the basis of the different lifetimes of the produced hadrons. Due to the relatively low cross sections and modest CST track reconstruction efficiency the decay length of the heavy hadrons is not reconstructed directly, but the DCA of tracks is used instead. The chosen heavy flavour tagging method also allows events with only 1 CST track to be used, for which it is not possible to reconstruct a secondary vertex. The DCA is defined as positive if the angle between the jet axis and the line joining the vertex to the point of DCA is less than $90°$, and is defined as negative otherwise. Tracks from the decays of long lived particles will mainly have a positive true DCA, whilst those produced at the primary vertex will have zero true DCA. Tracks reconstructed with negative DCA values mainly result from detector resolution.

Figure 4(a) shows the DCA distribution of CST tracks associated to the jet axis. The data are seen to be asymmetric with positive values in excess of negative values indicating the presence of long lived particles. The simulation gives a reasonable description of the data. The component of the simulation that arises from light quarks is almost symmetric at low DCA. The asymmetry at DCA $\gtrsim 0.1$ cm is mainly due to long lived strange particles such as K_s. The c component exhibits a moderate asymmetry and the b components shows a marked asymmetry. The differences are due to the different lifetimes of the produced hadrons. In order to reduce the effects of the strange component, a cut of |DCA| <0.1 cm is imposed on all tracks used in the analysis.

In order to optimise the separation of the quark flavours use is made of the significance [25], defined as the ratio of the DCA to its error. This distribution is shown for all tracks in figure 4(b), where a good description of the data by the simulation is observed apart from the tails, where the data are observed to lie above the simulation. For this reason, the significance distributions are only fitted in the range $-10 <$ significance < 10. A further optimisation is made by using different significance distributions for events with different multiplicities. The first significance distribution S_1 is defined for events where only 1 reconstructed CST track is linked to the jet, and is simply the significance of the track. The second significance distribution S_2 is defined for events with two or more tracks associated with the jet and is the significance of the track with the second highest absolute significance.

The S_1 and S_2 distributions are shown in figure 5. The distribution of S_2 gives a better separation power of light to heavy quarks, since for heavy quarks ≥ 2 tracks are usually produced with high significance, whereas for light quarks the chances of two tracks being produced at large significance due to resolution effects are small. Events with 1 CST track are retained to improve the statistical precision of the measurements.

In order to substantially reduce the uncertainty due to the DCA resolution and the light quark normalisation the negative bins in the S_1 and S_2 distributions are subtracted from the positive. The subtracted distributions are shown in figure 6. It can be seen that the resulting distributions are expected to be dominated by c quark events[2], with an increasing b fraction with increasing significance. The light quarks contribute around 15% or less for all values of significance.

4.4 Fit Procedure

The fractions of c, b and light quarks of the data, are extracted in each x–Q^2 interval using a simultaneous fit to the subtracted S_1 and S_2 distributions (as in figure 6) and the total number of

[2]Events that contain c hadrons via decay of b hadrons are not included in the definition of c quark events.

inclusive events before track selection, using the c, b and uds Monte Carlo samples as templates. A standard least squares fit is used. The Monte Carlo c, b and uds distributions in each x–Q^2 interval are allowed to be modified by the scale factors P_c, P_b and P_l, respectively. The χ^2 to be minimised in each interval is thus:

$$\chi^2 = \sum_{\mathrm{i}} \frac{\left(N_i^{\mathrm{data}} - P_c N_{ci}^{\mathrm{MC}} - P_b N_{bi}^{\mathrm{MC}} - P_l N_{li}^{\mathrm{MC}}\right)^2}{\sigma^2\left(N_i^{\mathrm{data}}\right) + \left(P_c \sigma\left(N_{ci}^{\mathrm{MC}}\right)\right)^2 + \left(P_b \sigma\left(N_{bi}^{\mathrm{MC}}\right)\right)^2 + \left(P_l \sigma\left(N_{li}^{\mathrm{MC}}\right)\right)^2}$$
$$+ \frac{\left(N_{\mathrm{tot}}^{\mathrm{data}} - P_c N_{\mathrm{tot}c}^{\mathrm{MC}} - P_b N_{\mathrm{tot}b}^{\mathrm{MC}} - P_l N_{\mathrm{tot}l}^{\mathrm{MC}}\right)^2}{\sigma^2\left(N_{\mathrm{tot}}^{\mathrm{data}}\right) + \left(P_c \sigma\left(N_{\mathrm{tot}c}^{\mathrm{MC}}\right)\right)^2 + \left(P_b \sigma\left(N_{\mathrm{tot}b}^{\mathrm{MC}}\right)\right)^2 + \left(P_l \sigma\left(N_{\mathrm{tot}l}^{\mathrm{MC}}\right)\right)^2}, \quad (1)$$

where the sum runs over all bins with significance < 10 in both the S_1 and S_2 histograms; N_i^{data} is the number of data events in each bin with corresponding error $\sigma(N_i^{\mathrm{data}})$; N_{ci}^{MC}, N_{bi}^{MC} and N_{li}^{MC} is the number of Monte Carlo c, b and light quark events in each bin respectively, with corresponding errors $\sigma(N_{ci}^{\mathrm{MC}})$, $\sigma(N_{bi}^{\mathrm{MC}})$ and $\sigma(N_{li}^{\mathrm{MC}})$; $N_{\mathrm{tot}}^{\mathrm{data}}$ is the total number of events in each x–Q^2 interval with corresponding error $\sigma(N_{\mathrm{tot}}^{\mathrm{data}})$; $N_{\mathrm{tot}c}^{\mathrm{MC}}$, $N_{\mathrm{tot}b}^{\mathrm{MC}}$ and $N_{\mathrm{tot}l}^{\mathrm{MC}}$ is the total number of c, b and light quark Monte Carlo events before track selection in each x–Q^2 interval respectively, with corresponding statistical errors $\sigma(N_{\mathrm{tot}c}^{\mathrm{MC}})$, $\sigma(N_{\mathrm{tot}b}^{\mathrm{MC}})$ and $\sigma(N_{\mathrm{tot}l}^{\mathrm{MC}})$. The first term of the χ^2 gives information on the P_c and P_b fractions from the difference in shape of the significance distributions, whilst the second term constrains the overall normalisation and, therefore, determines P_l.

The results of the fit to the complete data sample are shown in figure 6. The fits give acceptable χ^2 values for all x–Q^2 intervals and for the total. Consistent results, all within two standard deviations of the statistical error, are found when fitting different significance distributions, for example fitting the S_1 or S_2 distributions alone; fitting the highest absolute significance track distribution for all events; and fitting the distribution for the track with the third highest absolute significance. Consistent results are also obtained fitting the significance distributions without subtraction of the negative bins from the positive, and also when varying the range of significance to be fitted within the range < 8 to < 13.

The results are converted to a measurement of the differential c cross section using:

$$\frac{\mathrm{d}\sigma^{c\bar{c}}}{\mathrm{d}x\mathrm{d}Q^2} = \frac{\mathrm{d}\sigma}{\mathrm{d}x\mathrm{d}Q^2} \frac{P_c N_c^{\mathrm{MCgen}}}{P_c N_c^{\mathrm{MCgen}} + P_b N_b^{\mathrm{MCgen}} + P_l N_l^{\mathrm{MCgen}}}, \quad (2)$$

where $\mathrm{d}\sigma/\mathrm{d}x\mathrm{d}Q^2$ is the measured inclusive differential cross section from H1 [17] and N_c^{MCgen}, N_b^{MCgen} and N_l^{MCgen} are the generated number of c, b and light quark events from the Monte Carlo in each bin, respectively. A small ($\leq 5\%$) bin centre correction is applied using the NLO QCD expectation (see section 4.6) to convert the bin averaged measurement into a measurement at a single x–Q^2 point. The cross section is defined so as to include a correction for pure QED initial and final state radiative effects, but not electroweak corrections (see [17] for a more complete discussion).

The structure function $F_2^{c\bar{c}}$ is then evaluated from the expression

$$\frac{\mathrm{d}\sigma^{c\bar{c}}}{\mathrm{d}x\mathrm{d}Q^2} = \frac{2\pi\alpha^2}{xQ^4}((1 + (1-y)^2)F_2^{c\bar{c}} - y^2 F_L^{c\bar{c}}), \quad (3)$$

where the longitudinal structure function $F_L^{c\bar{c}}$ is estimated from the NLO QCD expectation[17]. The differential b cross section and $F_2^{b\bar{b}}$ are evaluated in the same manner. The maximum contribution of the longitudinal structure function is 2.3% of $F_2^{c\bar{c}}$ and 4.6% of $F_2^{b\bar{b}}$. It is also convenient to express the cross section as a 'reduced cross section' defined as

$$\tilde{\sigma}^{c\bar{c}} = \frac{\mathrm{d}\sigma^{c\bar{c}}}{\mathrm{d}x\mathrm{d}Q^2} \frac{xQ^4}{2\pi\alpha^2(1+(1-y)^2)}. \tag{4}$$

4.5 Systematic Errors

The sources of systematic uncertainty considered are as follows:

- A track efficiency uncertainty of $\pm 3.6\%$.
- An uncertainty in the DCA resolution of the tracks is estimated by varying the resolution in the Monte Carlo Simulation by an amount that encompasses the differences between the data and simulation. An additional Gaussian smearing of $200\ \mu\mathrm{m}$ to 5% of the tracks and $25\ \mu\mathrm{m}$ to the rest is introduced.
- A 4% uncertainty on the hadronic energy scale.
- An error on the jet axis is estimated by introducing an additional Gaussian smearing of $2°$.
- The uncertainty on the asymmetry of the light quark DCA is estimated by repeating the fits with the light quark S_1 and S_2 distributions (figure 6) set to zero.
- The uncertainties on the various D and B meson lifetimes, decay branching fractions and mean charge multiplicities are estimated by varying the input values of the Monte Carlo simulation by the errors on the world average measurements, or by adjusting the simulation to the world average value depending on which variation is larger. For the branching fractions of quarks to mesons and the lifetimes of the mesons the central values and errors on the world averages are taken from[8]. For the mean charged track multiplicities the values and uncertainties for c and b quarks are taken from MarkIII [26] and LEP/SLD [27] measurements, respectively.
- An uncertainty on the fragmentation function of the heavy quarks used in the Monte Carlo is estimated by repeating the fits with the Monte Carlo templates generated using the Peterson fragmentation function[28] with parameters $\epsilon_c = 0.058$ and $\epsilon_b = 0.0069$.
- An uncertainty on the bin centre correction leading to a 5% error on the measured cross section.
- An uncertainty in the QCD model of heavy quark production used in the Monte Carlo is estimated by using RAPGAP in a mode where heavy quarks are generated with a $1:1$ ratio of QPM to PGF induced events.

- Other sources of systematic error pertaining to the NC selection were also considered[17]: a 1.5% uncertainty on the luminosity measurement; an uncertainty on the scattered positron polar angle of 1–3 mrad and energy of 0.7–3.0% depending on the polar angle; a 0.5% uncertainty on the scattered positron identification efficiency; a 0.5% uncertainty on the positron track-cluster link efficiency; a 0.3% uncertainty on the trigger efficiency and a 1% uncertainty on the cross section evaluation due to QED radiative corrections.

The total systematic error is obtained by adding all individual contributions in quadrature and is around 15% for $\tilde{\sigma}^{c\bar{c}}$ and 25% for $\tilde{\sigma}^{b\bar{b}}$.

4.6 Results

The measurements of $F_2^{c\bar{c}}$ and $F_2^{b\bar{b}}$ are shown in figure 7 as a function of x for two values of Q^2. The H1 data for $F_2^{c\bar{c}}$ are compared with the results of the ZEUS collaboration [2], where the cross sections were obtained from the measurement of $D^{*\pm}$ mesons. The results of the two measurements for $F_2^{c\bar{c}}$ are in good agreement.

The data are also compared with the prediction from the H1 PDF 2000 fit[17] in which the c and b quarks are treated in the ZM-VFNS scheme. The QCD prediction is compatible with the data. There is no evidence for an excess of the b cross section compared with QCD predictions as has been reported in other analyses [4, 3, 6, 7]. The errors on the data do not yet allow the different QCD schemes (see section 2) to be distinguished.

The measurements are also shown figure 8 in the form of the fractional contribution to the total ep cross section:

$$f^{c\bar{c}} = \frac{\mathrm{d}\sigma^{c\bar{c}}/\mathrm{d}x\mathrm{d}Q^2}{\mathrm{d}\sigma/\mathrm{d}x\mathrm{d}Q^2}. \tag{5}$$

The b fraction $f^{b\bar{b}}$ is defined in the same manner. NLO QCD is found to give a good description of the data, as shown by comparison with the ZM-VFNS prediction from the H1 fit [17].

The c and b fractions and cross sections are also measured integrated over the range $Q^2 > 150\ \mathrm{GeV}^2$ and $0.1 < y < 0.7$. This is a more restricted range than for the differential measurements, in order to minimise the extrapolations, and the following values are found:

$$\sigma^{c\bar{c}} = 431 \pm 59 \pm 69\ \mathrm{pb}$$
$$\sigma^{b\bar{b}} = 45 \pm 11 \pm 11\ \mathrm{pb}$$

NLO QCD is found to agree well with the data. For example, the VFNS prediction from MRST [31] gives:

$$\sigma^{c\bar{c}} = 426\ \mathrm{pb}$$
$$\sigma^{b\bar{b}} = 47\ \mathrm{pb}.$$

5 Conclusion

The production of c and b quarks at HERA has been studied using precise tracking information from the H1 vertex detector. The inclusive c and b cross sections are measured using a technique based on the lifetime of the heavy quark hadrons. The measurements are made using all events containing tracks with vertex detector information eliminating the need for large model dependent extrapolations to the full cross section. The predictions from perturbative QCD are found to agree well with both the integrated and differential cross sections.

Acknowledgements

We are grateful to the HERA machine group whose outstanding efforts have made this experiment possible. We thank the engineers and technicians for their work in constructing and maintaining the H1 detector, our funding agencies for financial support, the DESY technical staff for continual assistance and the DESY directorate for support and for the hospitality which they extend to the non DESY members of the collaboration.

References

[1] C. Adloff *et al.* [H1 Collaboration], Z. Phys. C **72**, 593 (1996) [hep-ex/9607012];
J. Breitweg *et al.* [ZEUS Collaboration], Phys. Lett. B **407** (1997) 402 [hep-ex/9706009];
C. Adloff *et al.* [H1 Collaboration], Nucl. Phys. B **545**, 21 (1999) [hep-ex/9812023];
J. Breitweg *et al.* [ZEUS Collaboration], Eur. Phys. J. C **12** (2000) 35 [hep-ex/9908012];
C. Adloff *et al.* [H1 Collaboration], Phys. Lett. B **528** (2002) 199 [hep-ex/0108039].

[2] S. Chekanov *et al.* [ZEUS Collaboration], Phys. Rev. D **69** (2004) 012004 [hep-ex/0308068].

[3] S. Chekanov *et al.* [ZEUS Collaboration], hep-ex/0405069

[4] C. Adloff *et al.* [H1 Collaboration], Phys. Lett. B **467**, 156 (1999) [Erratum-ibid. B **518**, 331 (2001)] [hep-ex/9909029].

[5] J. Breitweg *et al.* [ZEUS Collaboration], Eur. Phys. J. C **18** (2001) 625 [hep-ex/0011081];
S. Chekanov *et al.* [ZEUS Collaboration], hep-ex/0312057.

[6] CDF Coll., F. Abe *et al.*, Phys. Rev. Let. 71 (1993) 2396, Phys. Rev. D 53 (1996) 1051;
D0 Coll., S. Abachi *et al.*, Phys. Rev. Let 74 (1995) 3548, Phys. Let. B 370 (1996) 239.

[7] M. Acciarri *et al.* [L3 Collaboration], Phys. Lett. B **503**, 10 (2001) [hep-ex/0011070].

[8] K. Hagiwara *et al.* [Particle Data Group Collaboration], Phys. Rev. D **66** (2002) 010001.

[9] H. L. Lai *et al.*, Phys. Rev. D **55** (1997) 1280 [arXiv:hep-ph/9606399].

[10] A. D. Martin, W. J. Stirling and R. G. Roberts, Phys. Rev. D **50** (1994) 6734 [hep-ph/9406315].

[11] E. Laenen, S. Riemersma, J. Smith and W. L. van Neerven, Nucl. Phys. B **392** (1993) 162;

E. Laenen, S. Riemersma, J. Smith and W. L. van Neerven, Nucl. Phys. B **392** (1993) 229;

S. Riemersma, J. Smith and W. L. van Neerven, Phys. Lett. B **347** (1995) 143 [hep-ph/9411431].

[12] F. I. Olness and W. K. Tung, Nucl. Phys. B **308** (1988) 813;

M. A. G. Aivazis, J. C. Collins, F. I. Olness and W. K. Tung, Phys. Rev. D **50** (1994) 3102 [hep-ph/9312319];

M. A. G. Aivazis, F. I. Olness and W. K. Tung, Phys. Rev. D **50** (1994) 3085 [hep-ph/9312318];

M. Kramer, F. I. Olness and D. E. Soper, Phys. Rev. D **62** (2000) 096007 [hep-ph/0003035];

S. Kretzer, H. L. Lai, F. I. Olness and W. K. Tung, hep-ph/0307022;

R. S. Thorne and R. G. Roberts, Phys. Rev. D **57** (1998) 6871 [hep-ph/9709442];

R. S. Thorne and R. G. Roberts, Phys. Lett. B **421** (1998) 303 [hep-ph/9711223];

R. S. Thorne and R. G. Roberts, Eur. Phys. J. C **19** (2001) 339 [hep-ph/0010344];

M. Cacciari, M. Greco and P. Nason, JHEP **9805** (1998) 007 [hep-ph/9803400];

M. Cacciari, S. Frixione and P. Nason, JHEP **0103** (2001) 006 [hep-ph/0102134].

[13] M. Buza, Y. Matiounine, J. Smith and W. L. van Neerven, Phys. Lett. B **411** (1997) 211 [hep-ph/9707263];

A. Chuvakin, J. Smith and W. L. van Neerven, Phys. Rev. D **61** (2000) 096004 [hep-ph/9910250];

A. Chuvakin, J. Smith and W. L. van Neerven, Phys. Rev. D **62** (2000) 036004 [hep-ph/0002011].

[14] I. Abt *et al.* [H1 Collaboration], Nucl. Instrum. Meth. A **386** (1997) 310 and 348.

[15] D. Pitzl *et al.*, Nucl. Instrum. Meth. A **454**, 334 (2000) [hep-ex/0002044].

[16] T. Nicholls *et al.* [H1 SPACAL Group Collaboration], Nucl. Instrum. Meth. A **374** (1996) 149.

[17] C. Adloff *et al.* [H1 Collaboration], Eur. Phys. J **C 30** (2003) 1-32 [hep-ex/0304003].

[18] R. Brun, R. Hagelberg, M. Hansroul and J. C. Lassalle, CERN-DD-78-2-REV.

[19] H. Jung, Comput. Phys. Commun. **86** (1995) 147.

[20] T. Sjostrand, Comput. Phys. Commun. **82** (1994) 74.

[21] A. Kwiatkowski, H. Spiesberger and H. J. Mohring, Comput. Phys. Commun. **69** (1992) 155.

[22] S. D. Ellis and D. E. Soper, Phys. Rev. D **48**, 3160 (1993) [hep-ph/9305266];

S. Catani, Y. L. Dokshitzer, M. H. Seymour and B. R. Webber, Nucl. Phys. B **406**, 187 (1993).

[23] C. Adloff *et al.* [H1 Collaboration], Z. Phys. C **74**, 221 (1997) [hep-ex/9702003].

[24] T. Ahmed *et al.* [H1 Collaboration], Phys. Lett. B **298**, 469 (1993).

[25] D. Buskulic *et al.* [ALEPH Collaboration], Phys. Lett. B **313** (1993) 535.

[26] D. Coffman *et al.* [MARK-III Collaboration], Phys. Lett. B **263** (1991) 135.

[27] D. Abbaneo *et al.* [LEP/SLD Heavy Flavour Working Group], LEPHF 2001-01, available from `http://lepewwg.web.cern.ch/LEPEWWG/heavy/`.

[28] C. Peterson, D. Schlatter, I. Schmitt, and P.M. Zerwas, Phys. Rev. D 27 (1983) 105.

[29] R. Frühwirth,et al., Nucl. Instrum. Meth. A **502**, 446 (2003).

[30] R. Frühwirth, A. Strandlie, Comput. Phys. Commun. 120 (1999) 197.

[31] A. D. Martin, R. G. Roberts, W. J. Stirling and R. S. Thorne, [hep-ph/0308087].

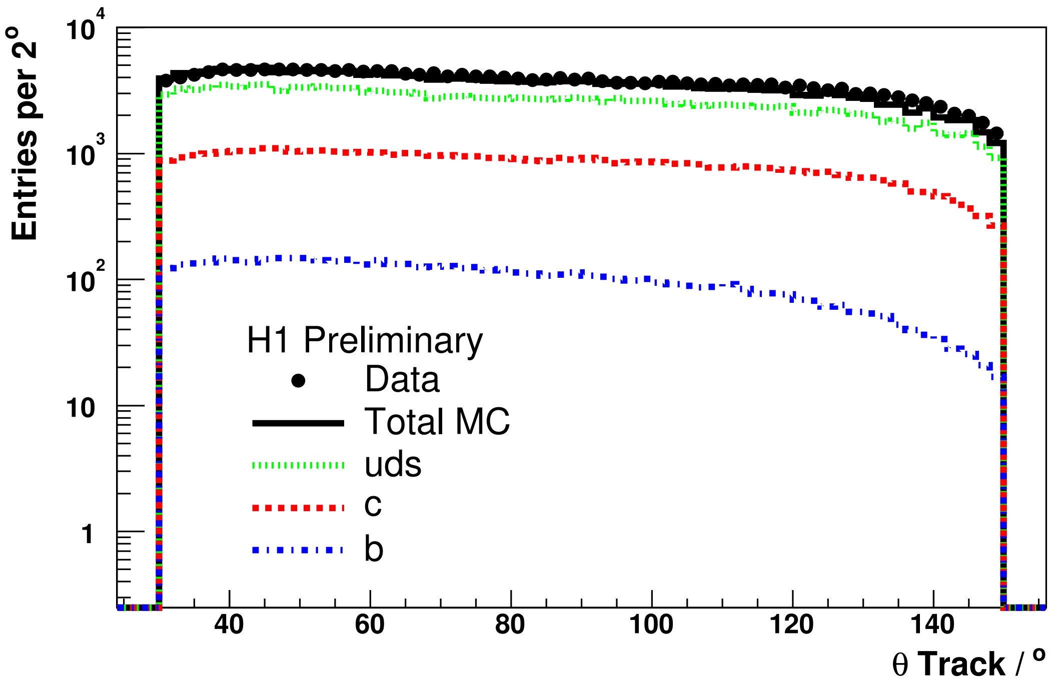

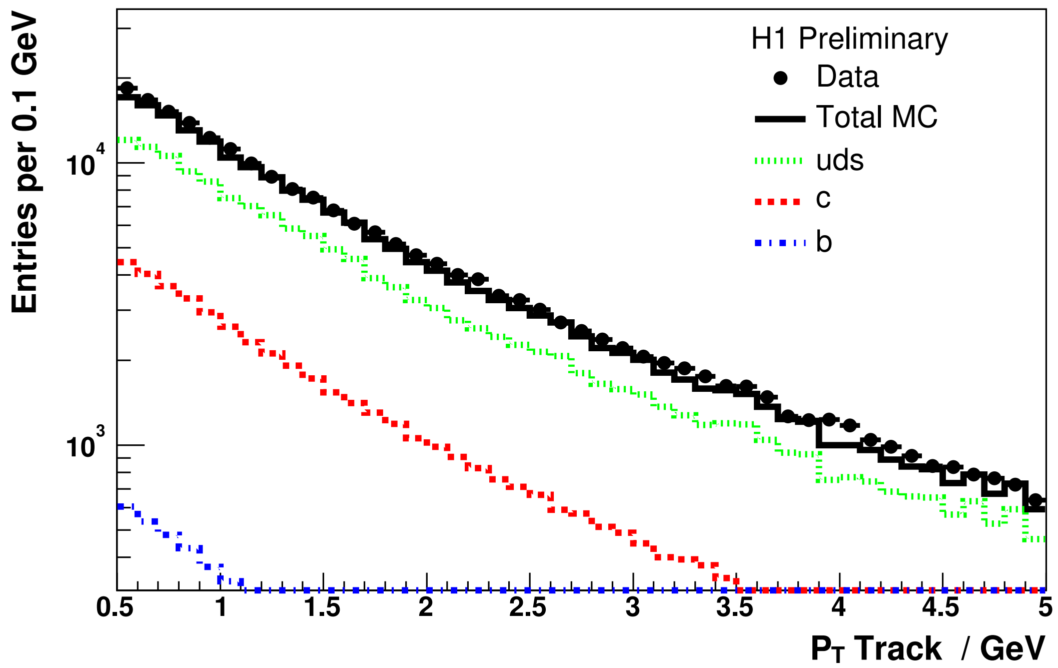

Figure 1: The polar angle distribution (a) and transverse momentum distribution (b) of all CST tracks. Included in the figure is the expectation from the RAPGAP Monte Carlo, showing the contribution from the various quark flavours after applying the scale factors obtained from the fit to the subtracted significance distributions of the data.

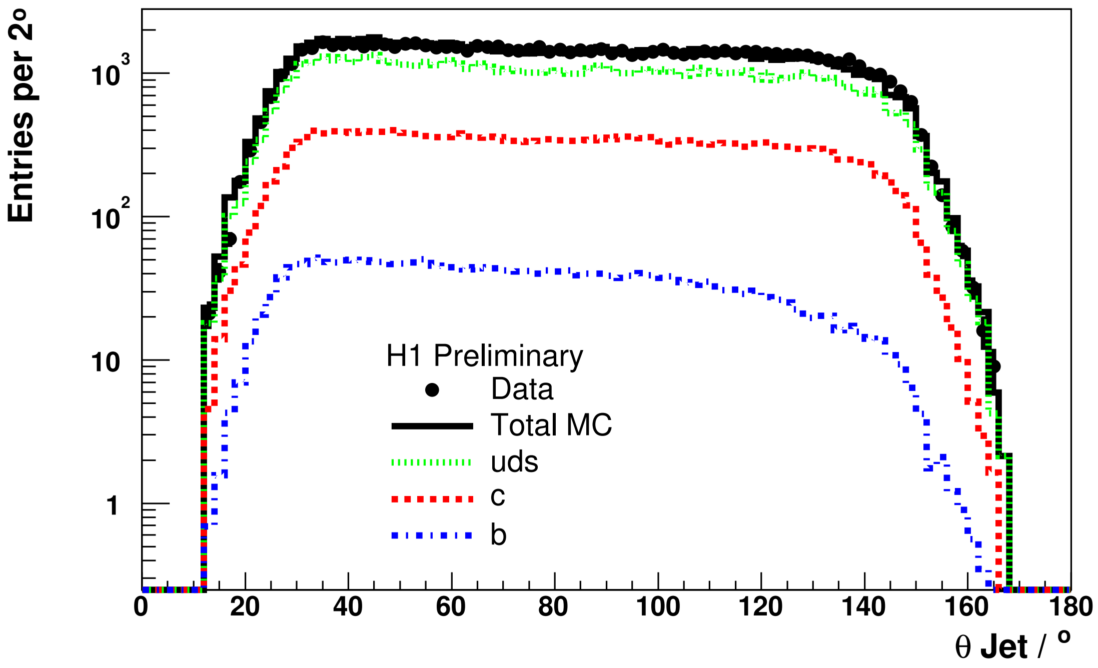

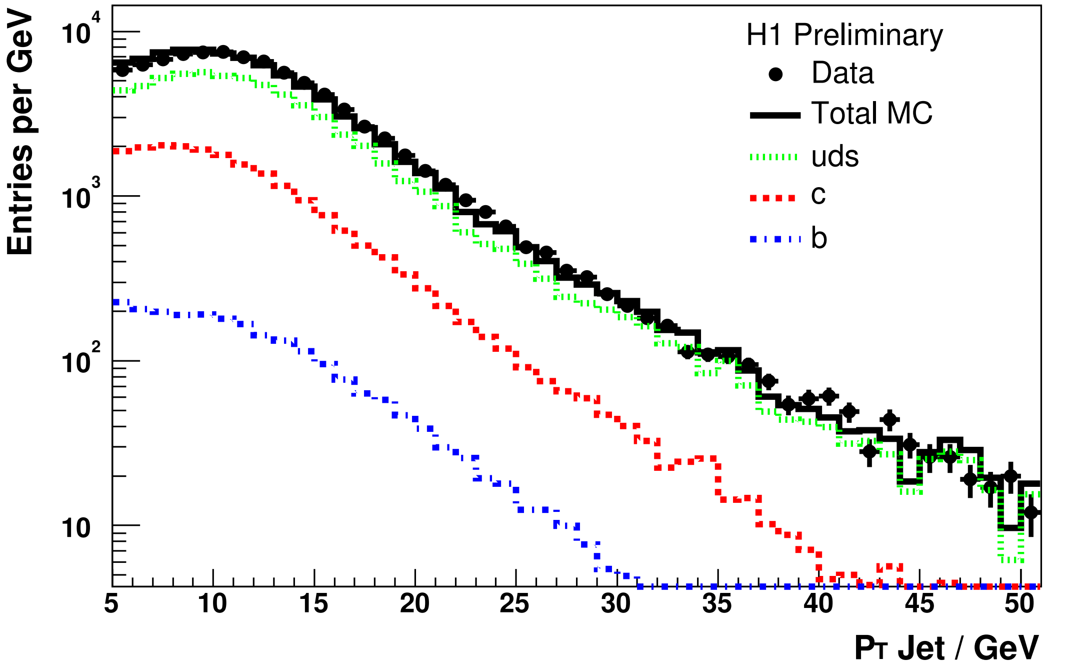

Figure 2: The polar angle distribution (a) and transverse momentum distribution (b) of the highest p_T jet which contains at least 1 reconstructed CST track within a cone of radius 1.0. If there are no reconstructed jets the complete hadronic final state is used to define the jet axis. Included in the figure is the expectation from the RAPGAP Monte Carlo after applying the scale factors obtained from the fit to the subtracted significance distributions of the data.

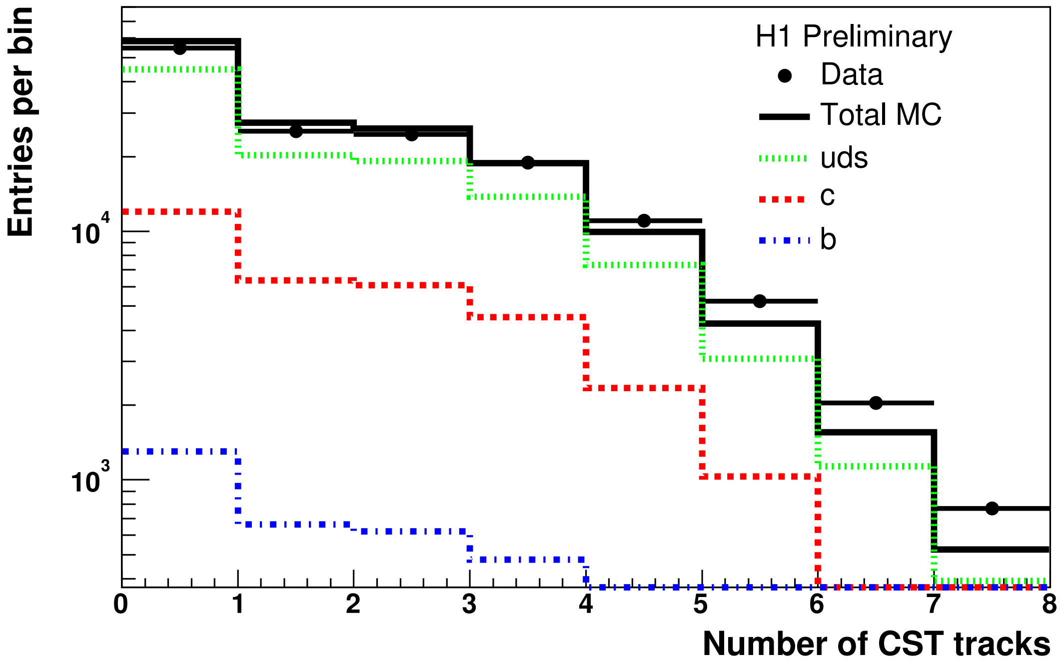

Figure 3: The number of reconstructed central silicon tracker (CST) tracks per event matched to the jet axis. Each CST track is required to have at least two CST hits and $p_T > 0.5$ GeV. Included in the figure is the expectation from the RAPGAP Monte Carlo, showing the contribution from the various quark flavours after applying the scale factors obtained from the fit of the subtracted significance distributions of the data (see section 4.4).

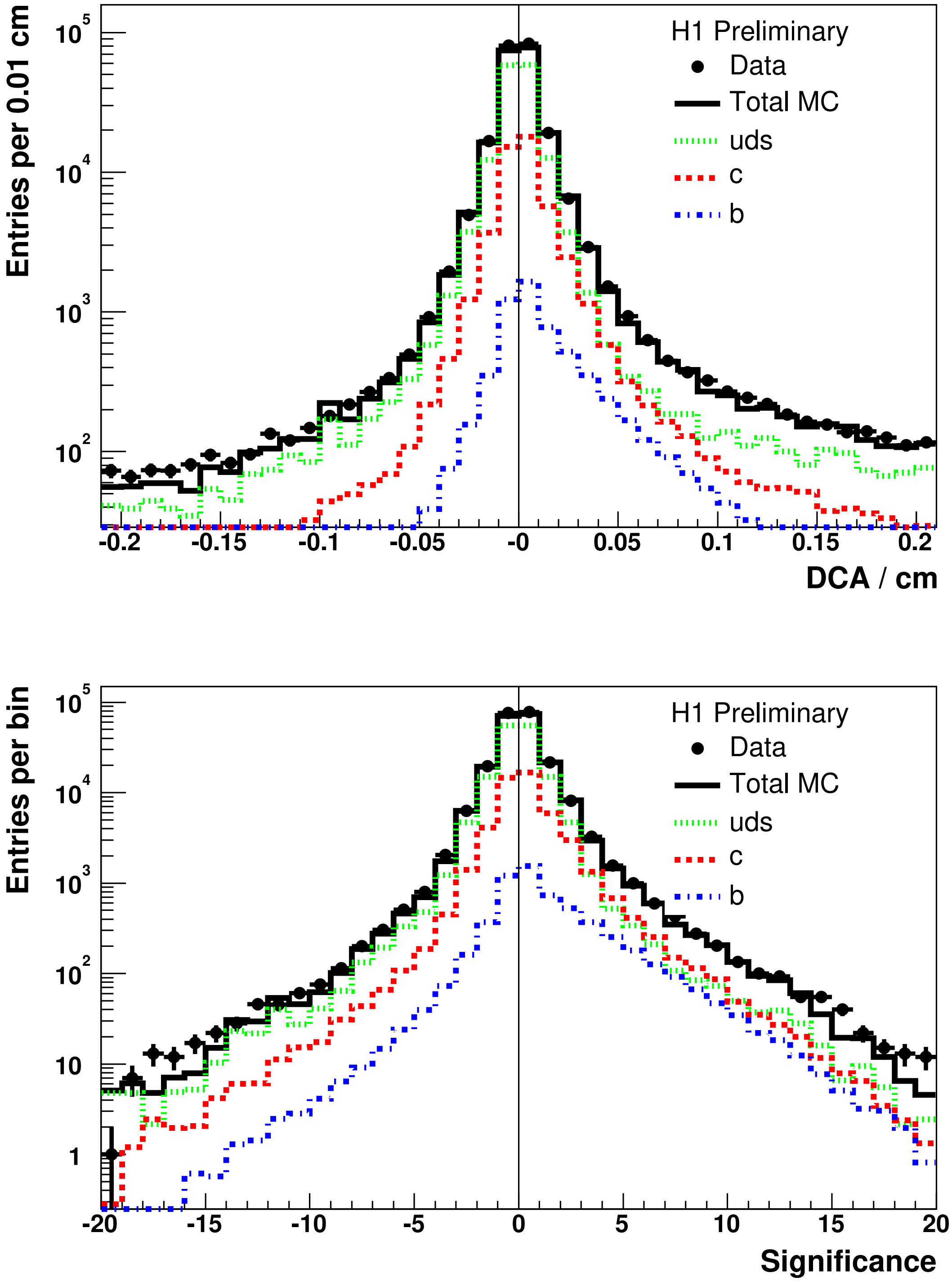

Figure 4: The distance of closest approach of a track to the vertex (DCA) in the x–y plane (a) and the signed significance (DCA/ σ (DCA) (b), where σ (DCA) is the error on the DCA, for all CST tracks. The cut $|\mathrm{DCA}| < 0.1$ cm has been applied in figure (b). Included in the figure is the expectation from the RAPGAP Monte Carlo, showing the contribution from the various quark flavours after applying the scale factors obtained from the fit to the subtracted significance distributions of the data.

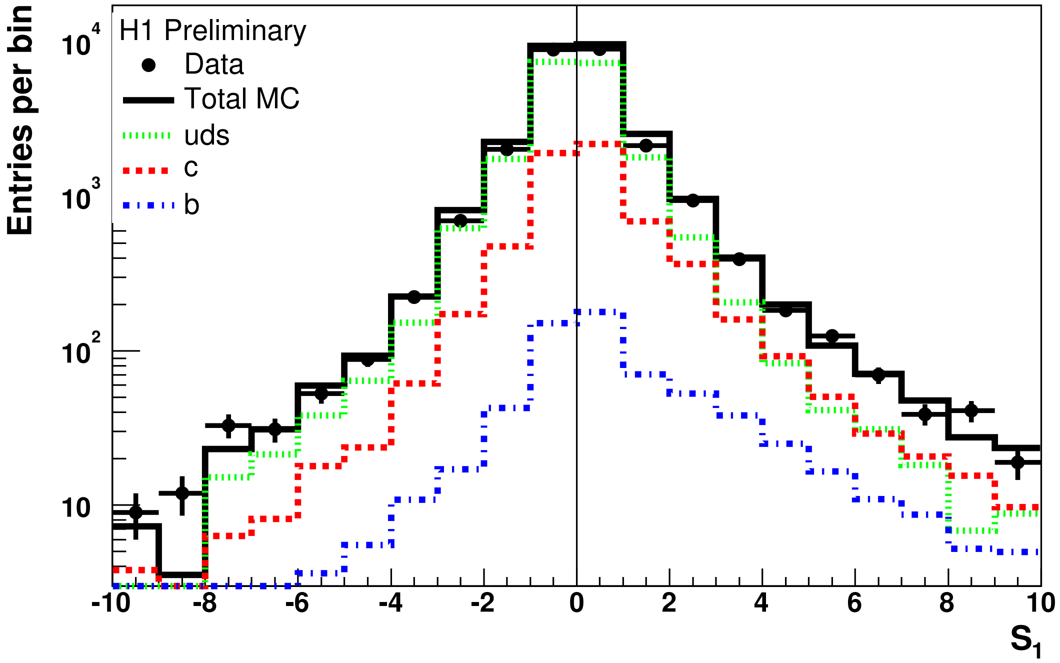

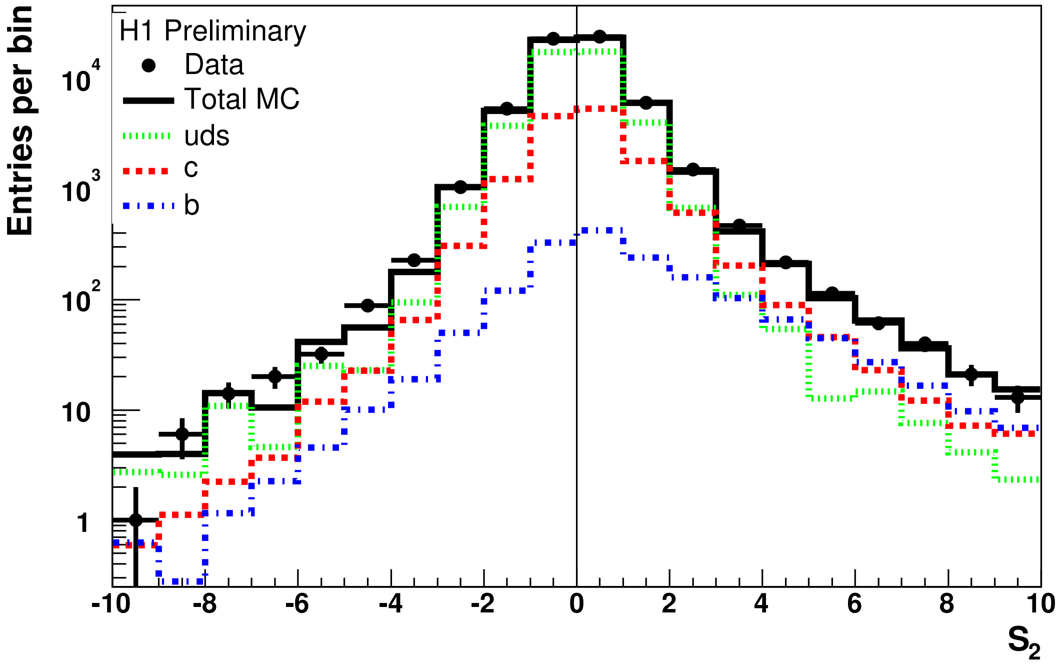

Figure 5: The signed significance $S_1 = DCA/\sigma(DCA)$ distribution per event (a) for events that contain 1 reconstructed CST track matched to the jet axis and the signed significance $S_2 = DCA/\sigma(DCA)$ distribution per event (b) of the track with the second highest absolute significance for events with ≥ 2 reconstructed CST tracks matched to the jet. Included in the figure is the expectation from the RAPGAP Monte Carlo, showing the contribution from the various quark flavours after applying the scale factors obtained from the fit to the subtracted significance distributions of the data.

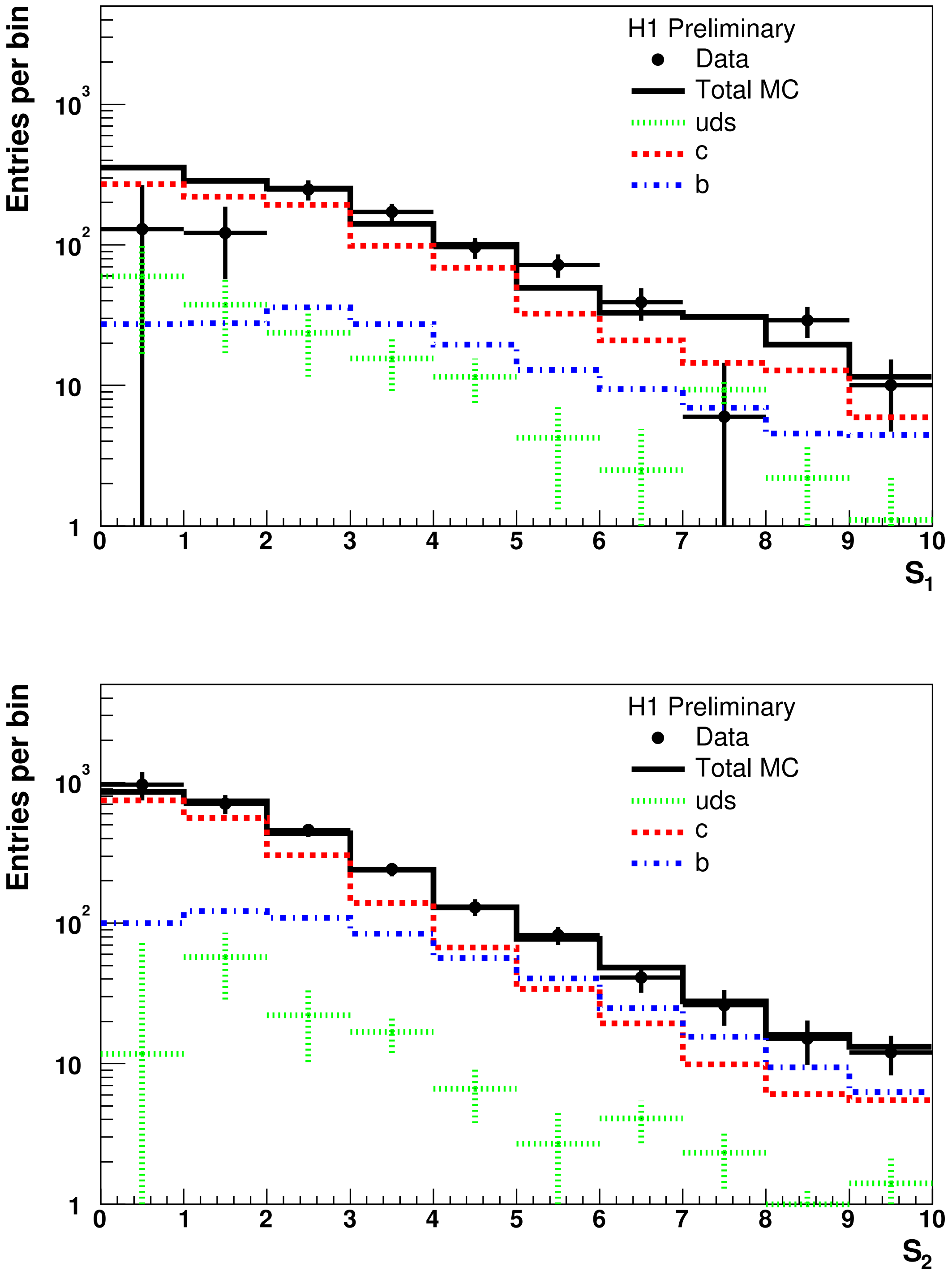

Figure 6: The distributions (a) S_1 and (b) S_2, after subtracting the bins with equal magnitude but negative sign from the positive. Included in the figure is the result from the fit to the data of the Monte Carlo distributions of events arising from c quarks or b quarks. The light quark contribution is also shown.

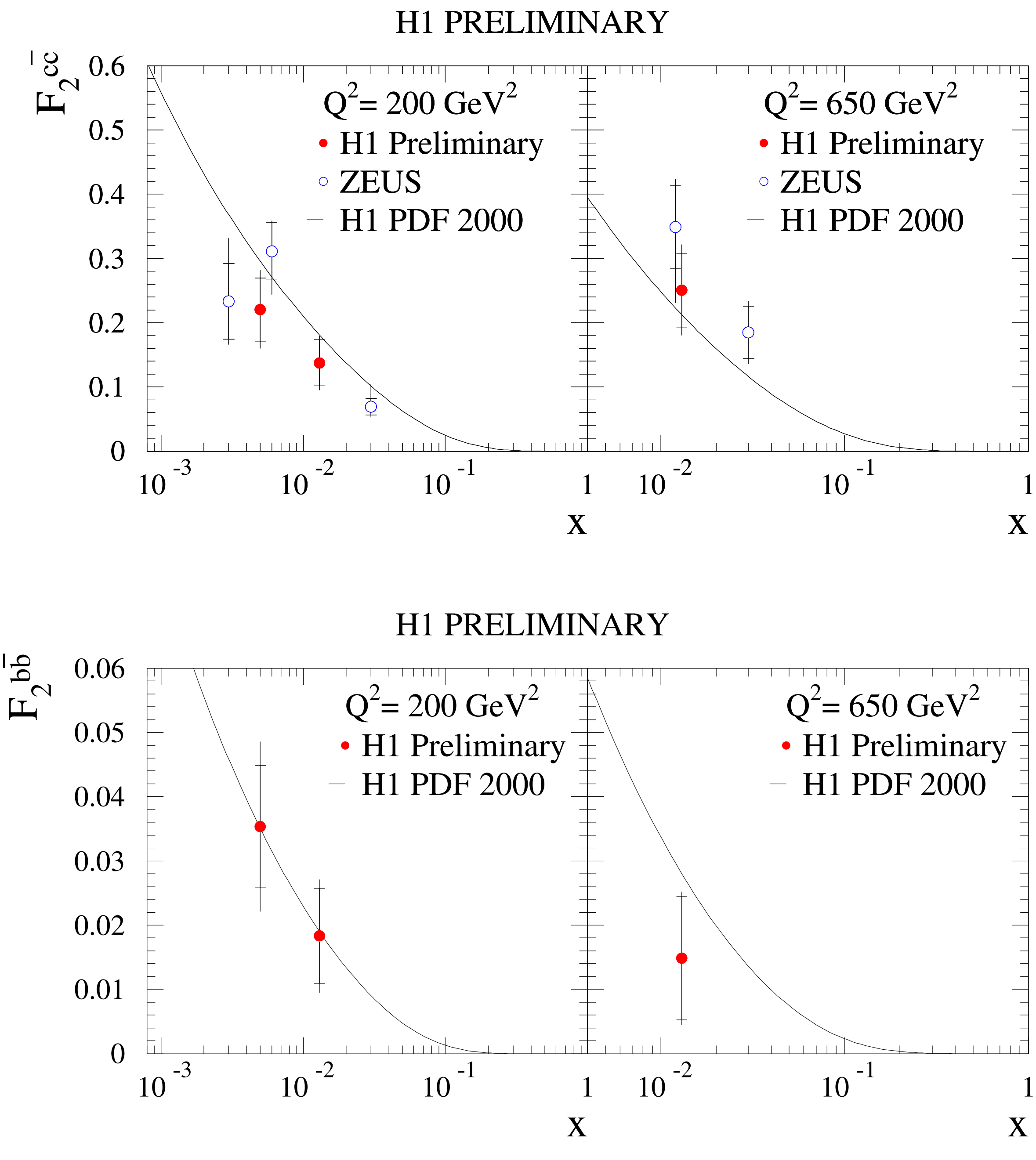

Figure 7: The measured $F_2^{c\bar{c}}$ (a) and $F_2^{b\bar{b}}$ (b) shown as a function of x for two different Q^2 values. The measurements of $F_2^{c\bar{c}}$ from ZEUS using D^*s to tag charm[2] and the prediction of a NLO QCD fit are also shown.

H1 PRELIMINARY

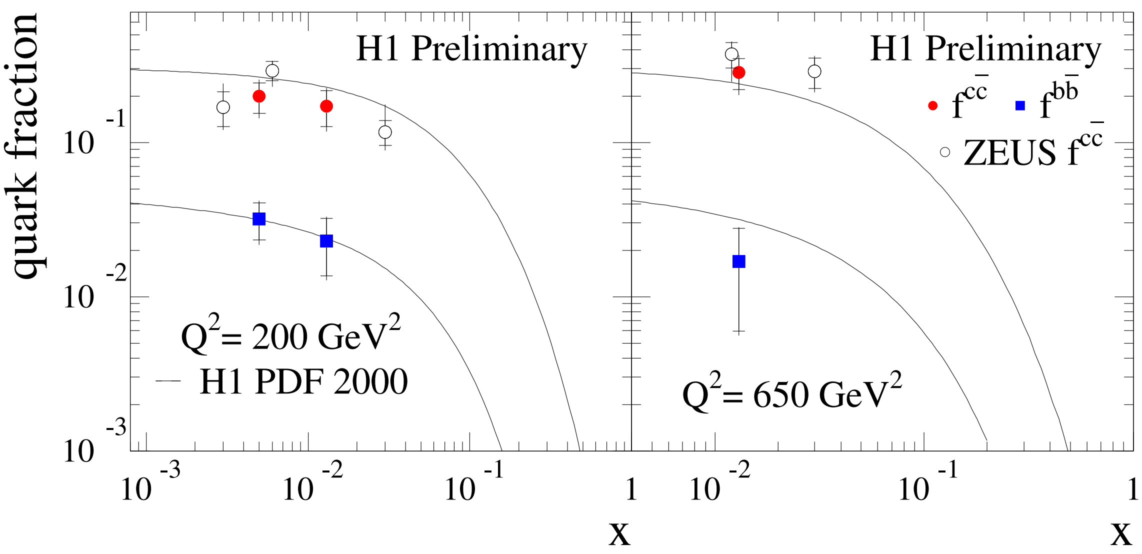

Figure 8: The ratio $f^{c\bar{c}}$ and $f^{b\bar{b}}$ shown as a function of x for two different Q^2 values. The measurements of $f^{c\bar{c}}$ from ZEUS using D^*s to tag charm[2] and the predictions of the H1 NLO QCD fit are also shown.